

PARAMETERIZATION OF INTERNAL WAVE BREAKING DUE TO NEAR-INERTIAL SHEAR

JULIE C. VANDERHOFF *

Brigham Young University, Provo, Utah

ABSTRACT

Internal waves are continuously being generated and propagating through the ocean and atmosphere. Internal wave breaking can occur far from generation sites, and the resultant mixing can transport momentum, heat, and pollutants across isopycnals, maintaining the energy balance in the ocean and preventing a stagnant deep ocean. But global circulation models cannot resolve these motions and they must be parameterized. For a completely accurate parameterization, all waves and their possible ensuing motions due to other waves, bottom topography, vortices, boundaries, etc. must be accounted for in the computations. Although many interactions are possible as internal waves propagate, evidence of constant large scale inertial motions in the ocean lead us to study the breaking of internal waves which propagate both aligned with and in opposition to large scale inertial waves. The results of the two types of interactions are dynamically different: one is a time-dependent critical level and the other a caustic interaction. These different types of interactions can lead to wave-breaking pre-or post-maturely due to the time-dependence of the inertial waves. The interaction is modeled through integration of the fully nonlinear, inviscid, Boussinesq equations of motion. In general, breaking is found to occur within a particular region of the inertial wave, which shifts for small scale waves that approach the interaction with different group velocities. Small-scale internal waves with the largest vertical wavelengths are most likely to break immediately as they enter an inertial wave propagating in the opposite direction, where the smallest vertical scale waves are more likely to break in-between strong refraction sites, if at all. When propagating the same direction, the scale separation between the waves is also important in determining breaking probability although in this case larger separation results in a higher probability of breaking. Wentzel-Kramers-Brillouin (WKB) ray tracing is used to supplement the fully nonlinear numerical model. These statistics expand the reach of calculations from the simulations and compare well with not only which waves are expected to break due to the time dependence, but also where they would be expected to break within the inertial wave, dependent on their properties. Results of the models also compare well with observations from the Hawaiian Ocean Mixing Experiment (HOME).

1. Introduction

Internal waves are ubiquitous in the ocean and can carry and dissipate energy throughout the ocean. Interactions with other flows can lead to internal wave steepening to a point of breaking, resulting in mixing of organisms, heat, and pollutants. This breaking and mixing must occur to keep the deep oceans from being stagnant and to close the basic energy balance. But locations of strong dissipation are not well known, nor are the specific mechanisms by which they occur. Vanderhoff, Nomura, Rottman, and Macaskill (2008) found small scale waves that propagate through larger scale inertial frequency waves with an initially

slow upward vertical group speed (slower than the upward phase speed of the long wave) and large vertical wavenumber have regions of greatly increased wave action during strong refraction. Breaking regions were not parameterized as a part of the study, though.

It is conjectured that mixing does not occur uniformly over the entire ocean, which has been supported by recent measurements which show an increase in mixing over topography (Polzin, Toole, Ledwell, and Schmitt (1997)). The Hawaiian Ocean-Mixing Experiment, HOME, (Pinkel, Munk, Worcester, Cornuelle, Rudnick, Sherman, Filloux, Dushaw, Howe, Sanford, Lee, Kunze, Gregg, Miller, Moum, Caldwell, Levine, an G. D. Egbert, Merrifield, Luther, Firing, Brainard, Flament, and Chave (2000), Pinkel and Rudnick (2006)) was conducted to examine the processes that lead to ocean mixing at a site of strong baro-

*Corresponding author address: Julie C. Vanderhoff, Mechanical Engineering Department, Brigham Young University, 435 CTB, Provo, UT, 84602-4201. (email: jvanderhoff@byu.edu).

clinic tidal generation (Noble, Cacchione, and Schwab (1988), Holloway and Merrifield (1999)). HOME had both observational and computational components. Through satellite altimetry, HOME researchers Zaron and Egbert (2006) found that 26 gigawatts of tidal energy is dissipated in the region of the Hawaiian Ridge. Some fraction of this radiates to the deep sea as low mode baroclinic waves while the remainder is dissipated locally (Rainville and Pinkel (2006a,b), Merrifield and Holloway (2002)). HOME observations demonstrated intense baroclinic wave generation, with high levels of turbulence in the lower 1500 m of the water column. Turbulent mixing rates decayed off-shore, and by 60 km away the rates had fallen to typical open-ocean values. Documenting the cascade process, by which barotropic tidal energy is transferred across a range of scales to eventual turbulent mixing, is a principal goal of HOME (Klymak, Moum, Nash, Kunze, Girton, Carter, Lee, Sanford, and Gregg (2006), Lee, Kunze, Sanford, Nash, Merrifield, and Holloway (2006), Klymak and Moum (2007a,b)).

The interaction of long and short internal waves plays a role in this process. Even though baroclinic tidal motions were most energetic at the Nearfield site, the shear is primarily associated with near inertial waves. Whether these waves are generated by the local wind, topographic interaction, or by non-linear interactions with the baroclinic tide is a subject of current research. Here, the HOME observations are used to set the scales of the inertial motions used in ray tracing and fully non-linear simulations of shorter waves propagating through longer inertial waves. The short waves are assumed to be pre-existing, with low initial energy, and their steepness is calculated as they propagate to assess locations of possible wave breaking.

The next section will cover the setup of each of the studied media: observations, numerical simulations, and ray tracing. In Section 3 results will be presented. Section 4 will draw conclusions about these results.

2. Setup

This section will cover the different setups of the observations, ray tracing calculations and numerical simulations.

a. Observational Setup

The HOME Nearfield experiment was conducted on the Kaena Ridge, a submerged extension of the Hawaiian island of Oahu. The Ridge extends west-north-west from Oahu for about 60 km, half of the distance to Kauaii. During September-October, 2002, the Floating Instrument Platform, FLIP, was moored as shown

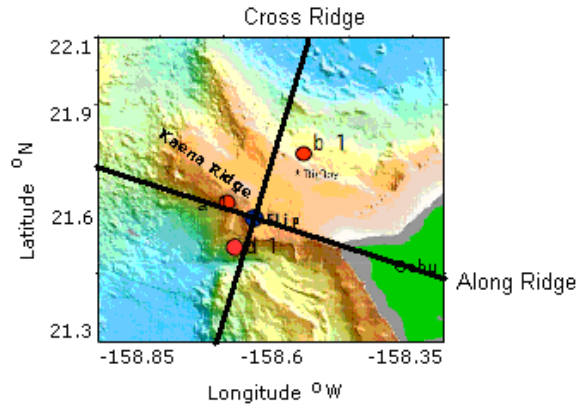


FIG. 1. Site of the 2002 HOME Nearfield Experiment. The blue circle represents the location of the Research Platform FLIP, the red circles are the locations of ancillary moorings. The solid lines denote cross-ridge and along-ridge directions.

in Fig. 1, 21.7° North, 158.6° West, on the south-west edge of the Ridge crest. At the location of FLIP the crest depth is about 1100 meters, with surrounding off-ridge areas at 5 km depth. Instruments deployed on FLIP, including an eight-beam, coded-pulse Doppler sonar that measured velocity from 50-800 m with 4m vertical resolution. Two CTDs (current-temperature-depth, Seabird SBE 911) profiled vertically from 20 meters to 820 meters depth at 4 minute intervals. The 3.5 m/s profiling speed leads to a resulting 1.1 meter vertical resolution in temperature, salinity and potential density. For further information of the setup of the experiment see Klymak, Pinkel, and Rainville (2007).

Slopes as steep as 1:4 define the north-north-east and south-south-west sides of the ridge. The ridge is oriented roughly normal to local semi-diurnal barotropic tidal flow. The S_2 (12 hour semidiurnal solar) tidal current has amplitude 2.8 cm/s East and 5.2 cm/s North. The K_1 (24 hour diurnal solar) tidal current has amplitude 3.2 cm/s East and 4.6 cm/s North. The M_2 (semidiurnal lunar - 12 hour 25 minute) tidal current has amplitude 6.4 cm/s East and 11.7 cm/s North, and is the dominant tide. It has a pronounced fortnightly cycle. Above 500 meters, energy and momentum fluxes are upward and southward (1 dyne/cm^2 during spring tide). Below 500 meters the fluxes are upward and northward. Above the ridge crest, power spectra of horizontal velocity and vertical displacement have pronounced D2 (semi-diurnal - 12 hour) peak. There is little evidence of a D2 peak in the shear, as shown later. The cruise covered two fortnightly cycles. The first neap tide was covered from year day 257 (Septem-

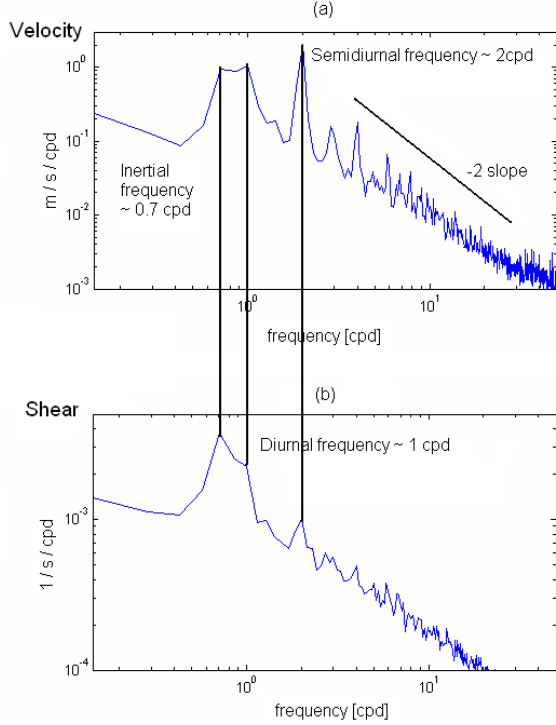


FIG. 2. Observations from sonar data over Kaena Ridge for one week (year day 260 to year day 267) over all depths (100 meters to 800 meters). Inertial, diurnal, and semidiurnal frequencies are labeled. A line with slope of -2 is superimposed on the frequency graph for the velocity. (a) Frequency spectrum for cross-ridge velocity averaged over all depths (371 data points). (b) Frequency spectrum for cross-ridge shear, U_z , averaged over all depths (371 data points).

ber 14, 2002) to year day 261 (September 18, 2002). The first spring tide was from year day 262 (September 19, 2002) to year day 269 (September 26, 2002).

Cross-ridge velocity and shear frequency spectra calculated over one week, from year day 260 to year day 267 for all depths are shown in Fig. 2. Peaks can be seen in the observations in both the velocity and shear frequency spectra at the inertial, diurnal, and semidiurnal frequencies. The strongest peak in the velocity corresponds to the tidal frequency, yet the strongest peak in the shear spectrum corresponds to the local inertial frequency - suggesting a strong inertial wave presence. An approximately -2 high frequency slope and high vertical wavenumber slope can also be seen.

Preliminary observational data taken on FLIP present a strong argument for a need to understand how the squared strainrate field $(\partial(\partial\zeta/\partial t)/\partial z = \partial^2\zeta/\partial z\partial t)$, which is a measure of high frequency

wave activity, is affected by the near-inertial waves. This can be seen in Fig. 3 a week-long record of the cross-ridge shear normalized by N and the strainrate squared, which represents high frequency wave activity. The sideways chevrons in the shear are characteristic of upward and downward propagating near-inertial waves, with periods of approximately 24 to 30 hours, frequency of about f to $1.3f$. Later, wave breaking regions with respect to these regions will be discussed.

b. The idealized problem

In the ray tracing and numerical simulations we consider the case of a packet of short waves approaching a single inertia packet either from above or below, as described in Vanderhoff, Nomura, Rottman, and Macaskill (2008), where a steady shear may be present as well. The coordinate system is (x, y, z) with z positive downward, x positive northward, and y positive eastward. We assume that the buoyancy frequency N and the Coriolis parameter f are both constant.

The inertial packet has wavenumber $\mathbf{K} = (0, 0, M)$, where $M = 2\pi/\lambda_i$ and λ_i is the vertical wavelength of the wave. The corresponding velocity field is uniform, horizontally, $\mathbf{u} = (u, v, 0)$, but confined in the vertical by a Gaussian envelope:

$$u + iv = u_0 e^{-z^2/2L^2} e^{i(Mz - ft)} \quad (1)$$

where L and u_0 are constants, real and complex respectively. The envelope of the inertia-wave packet assumed stationary, since the vertical component of the group velocity vanishes at the inertial frequency. The phases move vertically through the packet at speed $c = f/M$, assumed positive to match the observations analyzed. The short waves have wavenumber $\mathbf{k} = (k, 0, m)$, with k constant, and intrinsic frequency $\hat{\omega}$, which is the Doppler-shifted frequency, where

$$\hat{\omega}^2 = (N^2 k^2 + f^2 m^2)/(k^2 + m^2). \quad (2)$$

The vertical group velocity $c_g = \partial\hat{\omega}/\partial m$ is negative if m is positive and positive if m is negative.

The vertical displacement of the short waves is $\zeta = \zeta_0 \exp(i\theta)$, from which the wavenumber and wave frequency are given by $\mathbf{k} = \nabla\theta$ and $\omega = -\theta_t$, respectively, and where $\omega = \hat{\omega} + ku$. The wave-energy density E is related to ζ_0 by

$$E = \frac{1}{2} \rho_0 \zeta_0^2 N^2 \left[1 + \left(\frac{fm}{Nk} \right)^2 \right] \quad (3)$$

where ρ_0 is the mean density of the fluid.

The numerical simulations are initialized at time $t = 0$ with a short-wave packet whose vertical displacement field $\zeta(x, z, t)$ has the initial form

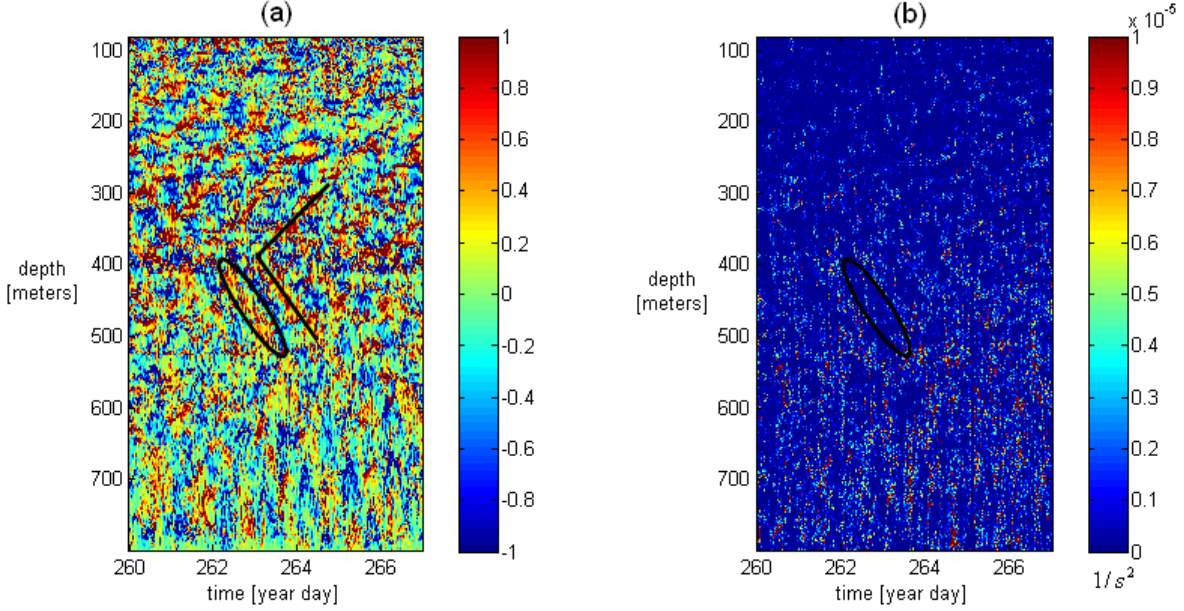


FIG. 3. (a) Cross-ridge shear normalized by buoyancy frequency, and presented in a reference frame moving vertically with isopycnal surfaces. (b) Strain rate squared [$1/s^2$] calculated from the profiling CTDs is also presented in this isopycnal following frame. The dark blue regions (circled) are relatively devoid of high-frequency waves.

$$\zeta(x, z, 0) = \text{Re} \left\{ \zeta_0 e^{-(z-z_0)^2/2\ell^2} e^{i(kx+mz)} \right\} \quad (4)$$

where ℓ and z_0 are real constants and ζ_0 is a complex constant. The initial vertical position z_0 is specified such that the short-wave packet is above the inertia-wave packet if $c_g < 0$, and below it if $c_g > 0$. The vertical derivative of the vertical displacement field is the wave steepness, derived from the dispersion relation and (3),

$$\zeta_z = -m \left| \left(\frac{2A\hat{\omega}}{\rho_0} \right)^{1/2} N^{-1} \right|. \quad (5)$$

When the wave steepness is greater than unity the short waves are expected to break.

For the ray tracing and numerical simulation results shown in this paper, we use the following ocean parameters, which are defined by the observations: $M = 2\pi/(100 \text{ m})$, $k = M/2$, $f = 10^{-4} \text{ s}^{-1}$, $N/f = 75$, and $u_0 = 0.05 \text{ m/s}$. For the numerical simulations, the initial steepness $|\zeta_z| = |m\zeta_0| = 0.1$, where subscript z represents the partial derivative with respect to z , $ML = \sqrt{2}\pi/10$, and $\ell/L = 0.75$. We will alter the vertical wavenumber, m , to realize different group speeds of the short wave.

c. Ray Theory

Using ray theory we can calculate approximately the behavior of the short wave encounter with the inertial wave group. To do this we assume that the inertial wave is both unaffected by the short wave interaction and has a much larger length scale than that of the short wave. Also we assume the short wave is determined by the linear dispersion relation. Then an evolution equation in characteristic form can be found for \mathbf{k} . For further detail see Vanderhoff et al. (2008).

1) THE RAY EQUATIONS

The ray-tracing results in this paper are obtained with the following pair of ray equations, for the vertical position of the ray path and the vertical wavenumber respectively:

$$\frac{dz}{dt} = c_g, \quad \frac{dm}{dt} = -k \frac{\partial u}{\partial z}. \quad (6)$$

Here $d/dt = \partial/\partial t + c_g \partial/\partial z$. Because the expression (1) has no dependence on x or y , the horizontal components $(k, 0)$ of the wavenumber of the short waves are conserved along the ray.

In a reference frame moving at the inertial-wave phase speed c , the inertial current appears steady. Solutions then exist for which the short-wave frequency in the inertial-wave reference frame

$$\Omega = \hat{\omega} + ku - cm \approx \text{constant}. \quad (7)$$

The trapped solutions have the short-wave group permanently confined within one wavelength of the inertia-wave, so that there are regions of the inertia-wave train where the short-wave group cannot propagate. The boundaries of these regions are called caustics and are the curves in (t, z) where neighboring rays cross (see Vanderhoff et al. (2008) Fig. 2). For our idealized model, caustics occur when

$$c_{gz} = C_z, \quad (8)$$

where the capitals represent the inertial wave. Critical levels occur when the relative frequency of the short wave goes to zero.

d. Numerical Simulations

Numerical results are obtained by integrating the fully nonlinear inviscid, Boussinesq equations of motion. In their vorticity-streamfunction form, these are:

$$\frac{\partial^2 \psi}{\partial x^2} + \frac{\partial^2 \psi}{\partial z^2} = q \quad (9)$$

$$\frac{\partial q}{\partial t} - J(\psi, q) - \frac{\partial \sigma}{\partial x} - f \frac{\partial v}{\partial z} = 0 \quad (10)$$

$$\frac{\partial v}{\partial t} - J(\psi, v) + fu = 0 \quad (11)$$

$$\frac{\partial \sigma}{\partial t} - J(\psi, \sigma) - N^2 w = 0, \quad (12)$$

where q is the y -component of vorticity and $J(\psi, q)$ the Jacobian with respect to (x, z) . Here the fluid velocity $\mathbf{u} = (u, v, w)$, and the stream function ψ is defined such that $u = \partial\psi/\partial z$, $w = -\partial\psi/\partial x$, and $q = \partial u/\partial z - \partial w/\partial x$. The scaled density perturbation due to the presence of internal wave motions is $\sigma = g\rho'/\rho_0$ where g is the acceleration due to gravity; the density $\rho = \rho' + \rho_0$, with $\rho_0(z)$ the mean density profile. Because of rotation, there is a nonzero v field, but all variables are assumed to be independent of y .

Periodic boundary conditions are imposed in both the x - and z -directions, and the equations are solved using a Fourier spectral collocation technique with Runge-Kutta time stepping. The computational domain contains one horizontal wavelength of the short waves in the horizontal direction and one or more vertical wavelength(s) of the inertia waves in the vertical direction. There are 512 grid points in the vertical direction, but only 16 grid points in the horizontal direction. The low horizontal resolution suffices for the wave propagation to an increased steepness, but does not resolve any breaking.

3. Results

Wave-breaking is defined when isopycnals are vertical, $\zeta_z > 1$, leading to overturning within the fluid and resulting turbulence. This can be calculated in the numerical simulations and observations by finding $\Delta\zeta/\Delta z$. For calculating wave steepness in ray theory equation (5) is used.

a. Wave Breaking in Observations

The observational results of calculating the breaking parameter, ζ_z , from the CTD data over two days and 200 meters depth are shown in Fig. 4b. The corresponding filtered inertial shear is shown in Fig. 4a. These results show a strong relationship between breaking and negative shear. Some of the strongest wave breaking regions are highlighted in Fig. 4. But what does the wavefield look like in these regions?

When low-frequency waves are filtered out, the average Reynolds stress (RS), uw , over two days is shown by the solid lines in Fig. 5. Upward propagating waves are on the left, and downward on the right. For upward propagating waves positive RS corresponds to wave propagation in negative- x , and for downward propagation, positive- x . The dashed lines are the average shear during breaking (5×10^3) over the two days. Both RS are near the same order, but each has a preferred direction during different sign shear breaking regions. In the upper region, where some of the strongest breaking regions occur, the downward waves have positive RS, corresponding to positive- x traveling waves. This directionality will become important while discussing the possible interactions leading to breaking.

Fig. 6 is an average of the RS over time at each depth multiplied by the shear and shown only in breaking regions. The data has been filtered to include only high frequency waves and Fig. 6a is upward propagating waves and Fig. 6b is downward propagating waves. Here, these are upward propagating waves and those propagating in the positive (northward) direction have a negative RS and are expected to break in negative shear regions (inertial wave horizontal velocity increasing as the short waves propagates upward), as well known critical layer theory shows. Those propagating southward have a positive Reynolds stress and are expected to break in positive shear regions. Thus, the product of the shear and RS should be positive in breaking regions. Regions in Fig. 6a where the product is negative are not explained by upward propagating waves interacting with the inertial wave. Thus the breaking mechanism should be due to downward propagating waves.

The downward propagating waves visualized in Fig. 6b includes both positive and negative product

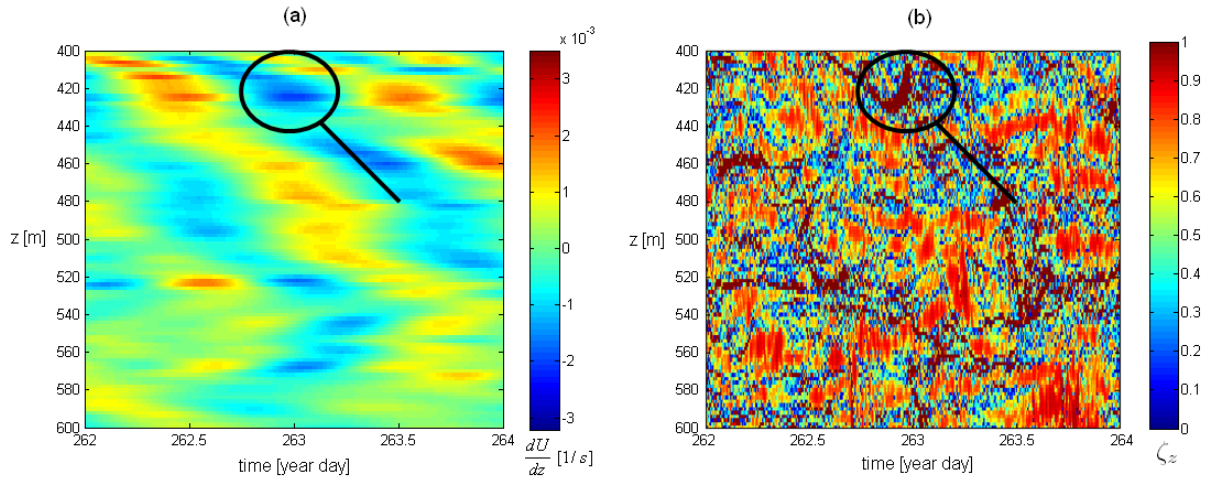


FIG. 4. Observational analysis over Kaena Ridge for two days over 200 meters depth. Circled regions of strongest breaking, with a line down another region of strong breaking. (a) Inertial shear divided by buoyancy frequency. (b) Wave breaking map calculated from CTD data. The colorbar represents ζ_z .

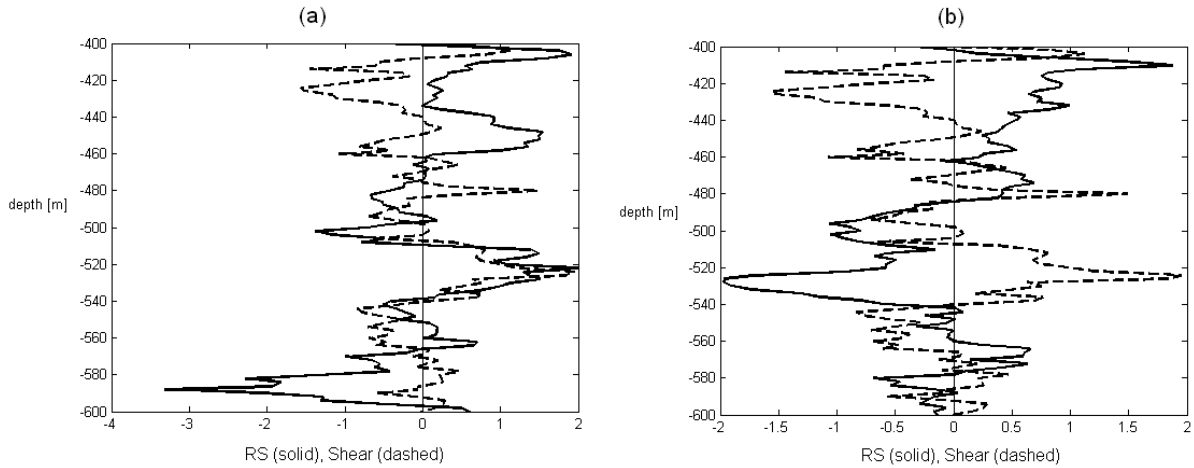


FIG. 5. Observational analysis over Kaena Ridge for two days over 200 meters depth. Reynolds stress, uw , $[m^2/s^2]$ (solid line) and shear $[1/s]$ ($\times 5 \times 10^3$) where breaking is occurring (dashed line) are each averaged over two days. (a) Filtered for upward propagating, high frequency waves only. (b) Filtered for downward propagating, high frequency waves only.

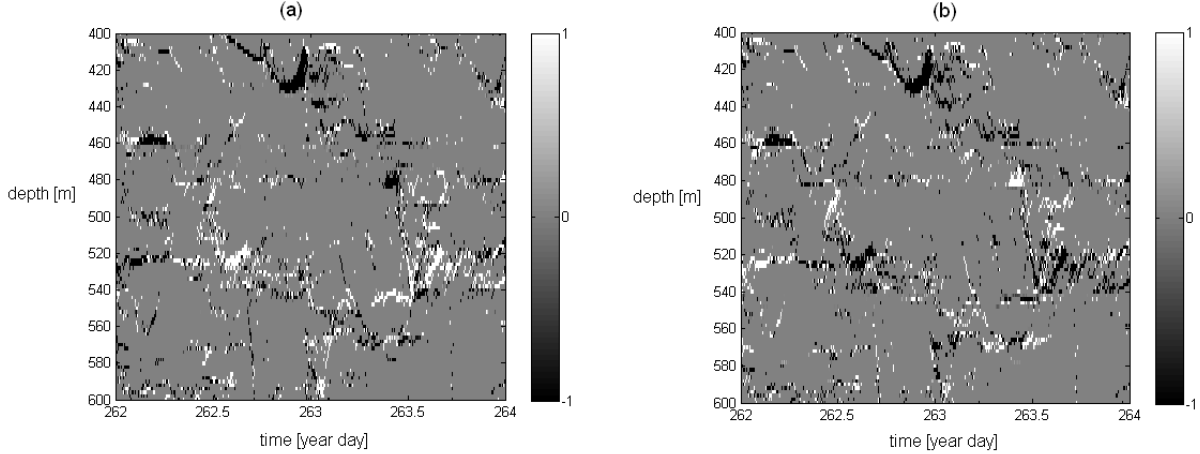


FIG. 6. Observational analysis over Kaena Ridge for two days over 200 meters depth. Reynolds stress (uw) is averaged over two days and multiplied by the shear at each point. Results are only shown where breaking is occurring. (a) Filtered for upward propagating, high frequency waves only. (b) Filtered for downward propagating, high frequency waves only. The colorbar represents a positive (white) or negative (black) product.

regions where the product was negative in Fig. 6a (where the upward traveling waves were not breaking). Specifically, the strong breaking region, circled in Fig. 4b, and the early time region near 460m depth, the product is negative. Fig. 5b shows in that spatial region, The RS is positive, meaning small-scale downward propagating waves are dominated by northward propagation. Although other interactions may also be occurring, this region was originally singled out due to the strong inertial wave presence, and thus the main breaking would be expected to be due to interactions between small-scale waves present and the large scale inertial wave. The goal of the next two subsections is to explain breaking in each region due to small-scale, high frequency wave interactions with an inertial wave.

Two types of interactions will be analyzed in an effort to understand the dynamics of the wave interactions in the observations. High-frequency, small-scale internal waves will interact with a large-scale inertial frequency wave with downward propagating phase speed, as is seen over depths of 400 meters to about 600 meters as discussed above. The small-scale waves will approach the inertial wave from above, below, and propagating in both positive- and negative-x directions. This should account for the main expected types of interactions in this region.

b. Wave Breaking in Ray Tracing

In an effort to explain the breaking phenomenon seen in the observations, ray tracing of small-scale internal waves are set to interact with an inertial wave with downward propagating phases.

Fig. 7 shows the ray lines, where locations of strong refraction are outlined by filled in ellipses, and the corresponding ζ_z values for a fast short wave. These values are estimated at the location of strong refraction, caustic, with the corrected amplitude. In ray tracing calculations the amplitude of the short wave approaches infinity as the caustic is approached and an Airy function relationship is used to estimate the maximum amplitude in this region. Locations of positive and negative shear which border the ellipses is shown in Fig. 7, where the upper left portion of the ellipse corresponds to positive background shear and the lower right portions correspond to negative background shear when the rays have a positive horizontal wavenumber, k . This is opposite for waves traveling in the negative x-direction (which have negative k values). In the lower portion of Fig. 7 there is a large increase in wave-steepness at the caustic, the steepness increases by over 15 times the original. Also, while traveling inbetween the phases the steepness reaches almost 15 times its original value. This first occurs in a region of positive shear, and thus breaking would first be expected in a region of positive shear. This results in the sign of the product of the Reynolds stress and the shear as positive, for both northward and southward, downward traveling short waves through an upward traveling inertial wave.

This will not be true for the downward propagating slower traveling waves in Fig. 8, which do not have the same first refraction seen in Fig. 7, but their steepness will begin to increase between the phases of the inertial wave. These waves may break after the first strong

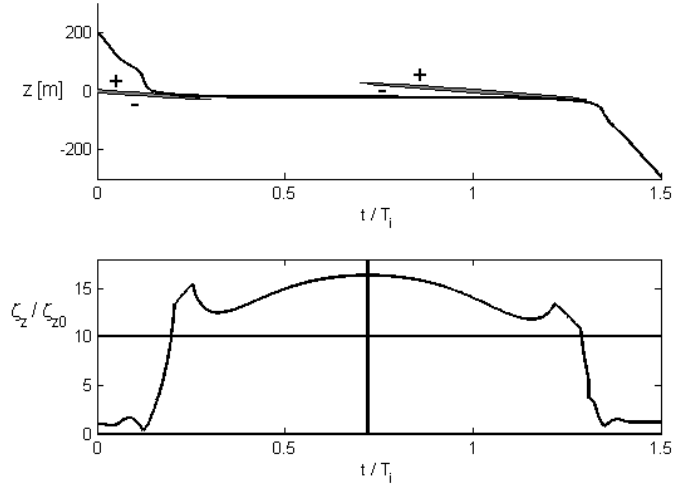


FIG. 7. Ray paths for a downward propagating short wave with a faster vertical group speed than the vertical phase speed of the inertial wave, $m/k = 3$. The waves are propagating in the positive- x direction, resulting in a positive Reynolds stress. The filled in ellipses are outlined by locations of strong refraction. The positive and negative signs depict the sign of the background shear at each location; positive above the strong refraction region, and negative below. Corresponding ζ_z/ζ_{z0} values along the ray are plotted below. If the initial steepness = 0.1, then the steepness is greater than 1 when the ratio of steepness to initial steepness = 10, where the horizontal line is drawn. The interaction is symmetric about the zero shear line (vertical line), but since the short wave reaches the max steepness in the region of positive shear first it may lose its energy in the positive shear region, leaving less energy and a smaller probability of breaking in the negative shear region. This is the only asymmetry in the short wave interactions, where breaking would be initiated. Negative- x traveling waves will have the opposite asymmetry.

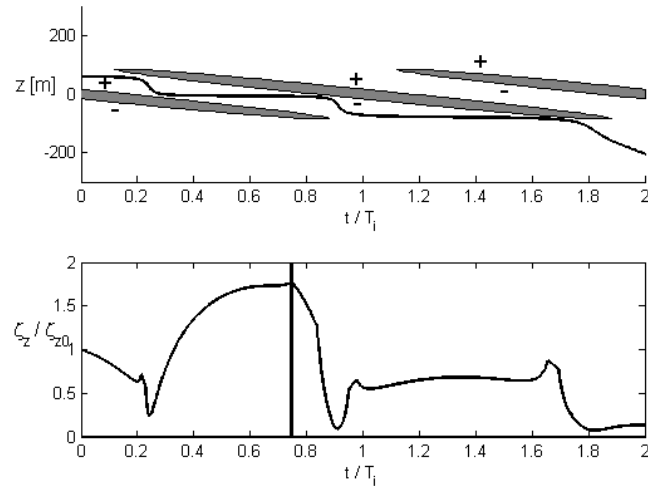


FIG. 8. As in Fig. 7, but for a short wave with a slower vertical group speed than the vertical phase speed of the inertial wave, $m/k = 35$.

refraction, in a positive shear region, or during the second in a negative shear region. Thus the product of the Reynolds stress and background shear during breaking may be either positive or negative. These, slower, small scale waves reaching caustics may explain the observations showing breaking when the sign of the Reynolds stress shear product is negative. These are some of the strongest breaking regions in the observations.

Waves propagating upward will not reach caustics, but will approach critical levels as they propagate. Steady critical levels have well known properties. Here, upward, northward traveling waves with a negative RS will approach a critical level and most likely break in regions of negative shear. Southward traveling waves have the opposite result, and therefore the same final product sign, positive. Thus, upward propagating waves are not expected to explain the regions in the observations which show a negative RS, shear product.

Short waves, approaching an inertial wave propagating in the same vertical direction, will most likely begin to break in a region where the horizontal velocity of the background increases in the direction of the horizontal short wave group speed as the short wave propagates vertically (critical level interaction). Thus if the z-direction is positive downwards, and short waves are propagating in the positive x-direction, as the background velocity becomes more positive as the short waves propagate in negative-z the short waves may break. This is a region of negative shear for a negative RS value. Fig. 9 displays the shear values when the breaking threshold is reached for 400 rays for fast (left) and slow (right) short waves. Short wave steepness is calculated and if it is greater than the threshold (steepness = 1) we assume it breaks and cut the amplitude down to 80% of the maximum for breaking. We let the waves propagate into the breaking region and cut them off at their maximum steepness. Then we kept this percent loss and calculated the total lost over the life of the wave. Sometimes it would break more than once. Note the product of the shear and Reynolds stress will be positive for all except case Fig. 9d. As expected from the theory and discussion of Fig. 5, slowly traveling downward, northward propagating waves with caustic interactions can explain the strong breaking regions in the observations.

c. Wave Breaking in Numerical Simulations

A wave breaking map for the numerical simulation of a small-scale, fast propagating wave approaching an inertial wave from below is shown in Fig. 10b, where the initial wave steepness is $\zeta_z = 0.8$. Next to it, Fig. 10a, is the corresponding background wave

shear field. In this setup, where the short waves are traveling upward in the positive x-direction (negative Reynolds stress), breaking will be in regions where the background shear is decreasing with increasing depth (negative shear): the region within the background phase where a critical level begins to be approached. These waves are the same type as in Fig. 9a. Slowly traveling waves (as in Fig. 9b) have the same result, although the approach to the critical level occurs sooner. Testing a few different waves, allowing the maximum background velocity and the initial steepness to change, about 70-90% of breaking for occurs in the expected negative shear, resulting in a positive shear, RS product. Since short-waves traveling upward in the negative-x direction (positive RS) break in positive shear regions, they also have the most breaking in regions of a positive shear, RS product. They are not shown here because the propagation dynamics are the same.

Fig. 11 shows the interaction when fast traveling downward propagating short waves interact with the inertial wave. Completely different dynamics are occurring where strong refraction dominates the interaction instead of critical levels (Vanderhoff et al. (2008), Sartelet (2003a,b)). An estimate of breaking from this interaction shows 90% of the breaking is occurring in regions of positive shear. This again results in a positive shear, RS product, and can describe some of the breaking regions in Fig. 6b with positive products which corresponded to negative products in Fig. 6a (regions where upward propagating waves most likely do not support breaking). Again, signs are opposite when short waves are propagating in the negative-x direction, thus the dynamics and final product sign are the same. Although this explains more of the breaking regions within the inertial wave, breaking occurring during the negative sign product of shear and RS has not yet been described.

The final possibility for breaking in these regions (assuming the main interactions here are between small-scale high-frequency waves and a large scale inertial wave) is the slowly traveling downward propagating waves of Fig. 9d and Fig. 5. Numerical simulations of this interaction are shown in Fig. 12. Breaking here occurs partially in regions of positive shear, and partially in regions of negative shear. Initially breaking is in regions of positive shear, but as the wave continues through the interaction it begins to break in negative shear regions as well. This interaction can describe the final breaking regions within the observations, where the product of the shear and RS is negative. In the region of strong breaking, RS was positive from Fig. 5 (downward, positive-x traveling as in

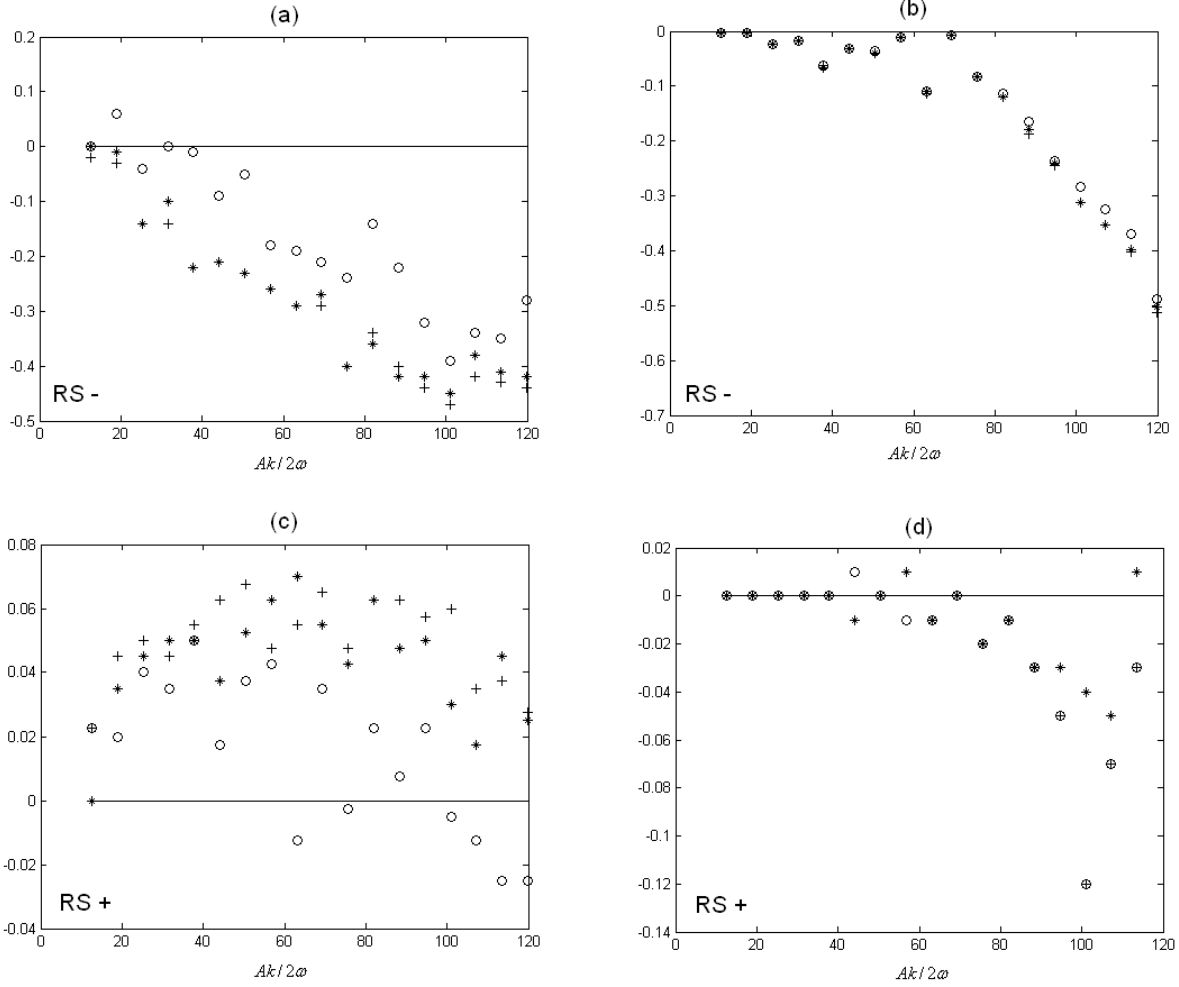


FIG. 9. Small-scale waves propagating through an inertial wave with phases propagating downward as in the ocean region. Shear values when breaking threshold is reached (open circle), at the max of the breaking region (cross), and at the final location of breaking (asterisk), for different values of initial steepness, $(Ak/\hat{\omega})^{1/2}$. After breaking the short wave has 80% of the energy it had when it reached the breaking threshold. If the shear is positive it is assigned a value of +1 and if negative it is -1. These values are averaged over 400 rays started at different initial slopes and depths. All small-scale waves are propagating in the positive-x direction. (a) Small-scale waves propagating upward with fast vertical group speed. Reynolds stress is negative. (b) Small-scale waves propagating upward with slow vertical group speed. Reynolds stress is negative. (c) Small-scale waves propagating downward with fast vertical group speed. Reynolds stress is positive. (d) Small-scale waves propagating downward with slow vertical group speed. RS is positive. Note the product of the shear and Reynolds stress will be positive for all except case (d)

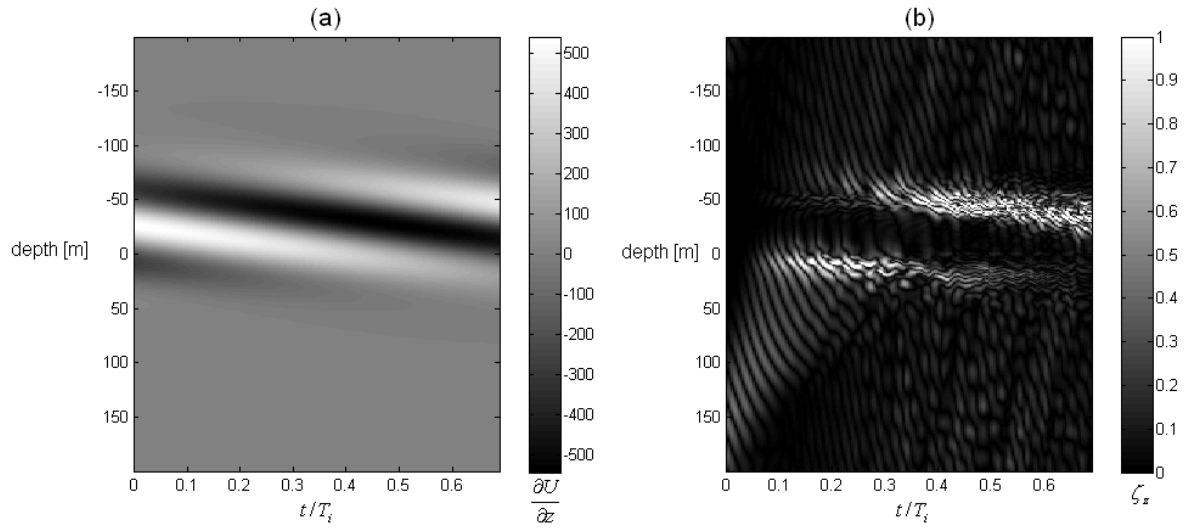


FIG. 10. Numerical simulation of a small-scale wave approaching an inertial wave from below. The vertical group speed of the small-scale wave is much faster than the downward vertical phase speed of the inertial wave, initially $m/k = -3$ (negative RS), and $\zeta_z = 0.8$. (a) Background shear [1/days]. (b) Possible breaking map. The colorbar represents ζ_z . Notice most of the breaking occurs in regions of negative shear.

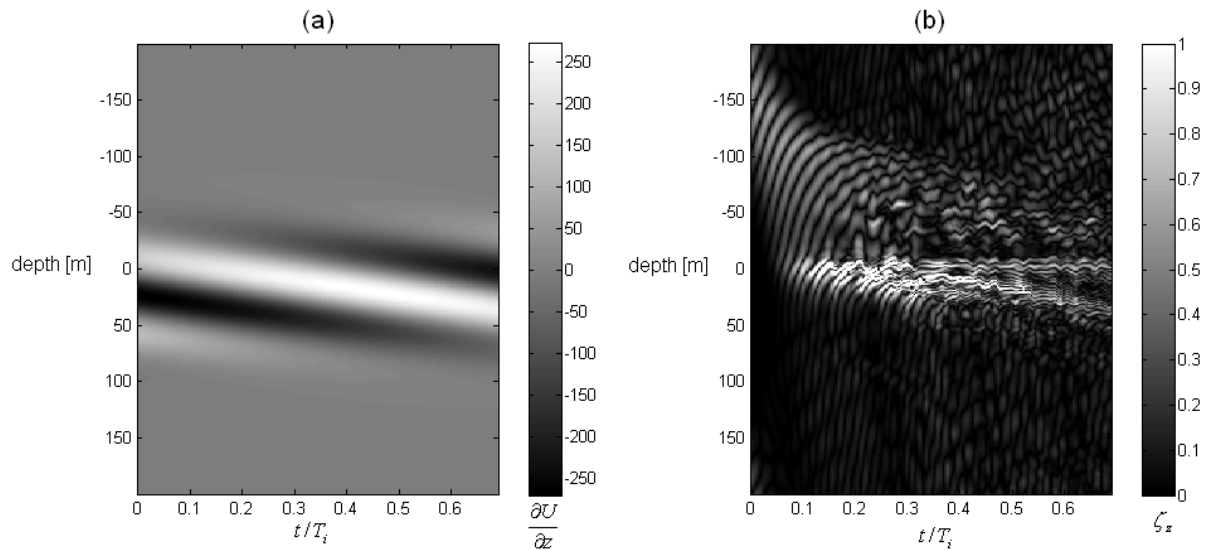


FIG. 11. As in Fig. 10, but short wave approaching from above, RS positive.

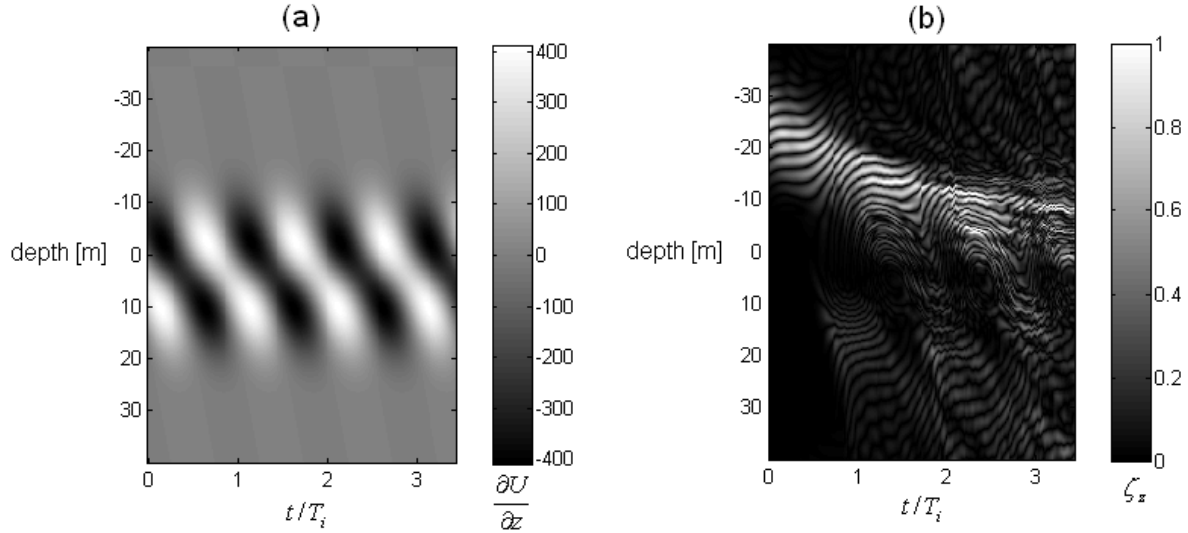


FIG. 12. As in Fig. 11, but short wave approaching slowly from above, RS positive.

Fig. 12) and shear was negative, resulting in a negative product and the same type of waves seen here. Fig. 2 also shows the frequency spectrum, where there is more wave energy at lower, high-frequencies, which are these slower traveling waves.

4. Discussion

The results shown here have given us insight into one of the possible mechanisms of short wave breaking in the ocean. This is when small-scale, high-frequency internal waves propagate upward and downward through the ocean and interact with constantly present large-scale inertial waves. Observations have shown these phenomenon occurring, and this analysis of small-scale, large-scale wave-wave interactions can describe the breaking phenomenon seen. Strong breaking was found in regions of negative shear. Small-scale waves propagating in all directions were present, with the lowest of the high-frequency waves being prominent. Locations where upward traveling waves cannot explain the shear at breaking locations, downward traveling waves are dominated by northward propagating waves which explain breaking in negative shear regions due to strong refraction zones only found within a propagating inertial wave. Other locations of breaking unexplainable by a conventional critical level analysis can be explained by downward propagating waves in the southward direction strongly refracting in negative shear locations. Ray tracing supports the analysis through a statistical analysis of many representative wave-wave interactions.

These types of wave-wave interactions may oc-

cur anywhere in the ocean where small-scale internal waves and inertial waves are present. Although in the region studied here, just over topography, there is much high-frequency internal wave activity due to the tidal flow over the topography, internal waves can be present in any area where the ocean is stratified (all but the upper mixed layer mainly). Inertial waves are large scale and have been observed as a regular phenomenon. Thus breaking due to these interactions may also provide insight into mixing occurring in the deep ocean and far from strong internal wave generation sites.

More analysis of other specific observational regions is suggested for a more full understanding of the processes dominating the breaking. These results were calculated with two-dimensional simulations and theory, yet three-dimensional simulations would be more accurate as the short waves begin to become unstable and are necessary to quantify wave breaking. It is also noted that the argument put forth here is not stating these are the only types of interactions occurring, but that they are highly probable and comparable.

REFERENCES

- Holloway, P. E., and Merrifield, M. E., 1999: Internal tide generation by seamounts, ridges, and islands. *J. Geophys. Res.*, **104**, 25,937–25,951.
- Klymak, J. M., and Moum, J. N., 2007a: Oceanic isopycnal slope spectra: Part I - Internal waves. *J. Phys. Oceanogr.*, **37**, 1215–1231.
- Klymak, J. M., and Moum, J. N., 2007b: Oceanic isopycnal slope spectra: Part II - Turbulence. *J. Phys. Oceanogr.*, **37**, 1232–1245.

- Klymak, J. M., Moum, J. N., Nash, J. D., Kunze, E., Girton, J. B., Carter, G. S., Lee, C. M., Sanford, T. B., and Gregg, M. C., 2006: An estimate of tidal energy lost to turbulence at the Hawaiian ridge. *J. Phys. Oceanogr.*, **36**, 1148–1164.
- Klymak, J. M., Pinkel, R., and Rainville, L., 2007: Direct breaking of the internal tide near topography: Kaena Ridge, Hawaii. *J. Phys. Oceanogr.*, in press.
- Lee, C. M., Kunze, E., Sanford, T. B., Nash, J. D., Merrifield, M. A., and Holloway, P. E., 2006: Internal tides and turbulence along the 3000-m isobath of the Hawaiian Ridge. *J. Phys. Oceanogr.*, **36**, 1165–1183.
- Merrifield, M. A., and Holloway, P. E., 2002: Model estimates of m2 internal tide energetics at the Hawaiian Ridge. *J. Geophys. Res.*, **107**, 3179–3191.
- Noble, M., Cacchione, D. A., and Schwab, W. C., 1988: Observations of strong mid-pacific tides above Horizon Guyot. *J. Phys. Oceanogr.*, **18**, 1300–1306.
- Pinkel, R., Munk, W., Worcester, P., Cornuelle, B. D., Rudnick, D., Sherman, J., Filloux, J. H., Dushaw, B. D., Howe, B. M., Sanford, T. B., Lee, C. M., Kunze, E., Gregg, M. C., Miller, J. B., Moum, J. M., Caldwell, D. R., Levine, M. D., and G. D. Egbert, T. B., Merrifield, M. A., Luther, D. S., Firing, E., Brainard, R., Flament, P. J., and Chave, A. D., 2000: Ocean mixing studied near Hawaiian Ridge. *Eos, Trans. Am. Geophys. U.*, **81**, 545–553.
- Pinkel, R., and Rudnick, D., 2006: Introduction to a series of papers from the Hawaiian Ocean Mixing Experiment. *J. Phys. Oceanogr.*, **36**, 965–966.
- Polzin, K. L., Toole, J. M., Ledwell, J. R., and Schmitt, R. W., 1997: Spatial variability of turbulent mixing in the abyssal ocean. *Science*, **276**, 93–96.
- Rainville, L., and Pinkel, R., 2006a: Baroclinic energy flux at the Hawaiian Ridge: Observations from the R/P FLIP. *J. Phys. Oceanogr.*, **36**, 1104–1122.
- Rainville, L., and Pinkel, R., 2006b: Propagation of low-mode internal waves through the ocean. *J. Phys. Oceanogr.*, **36**, 1202–1219.
- Sartelet, K. N., 2003a: Wave propagation inside an inertia wave. Part I: Role of time dependence and scale separation. *J. Atmos. Sci.*, **60**, 1433–1447.
- Sartelet, K. N., 2003b: Wave propagation inside an inertia wave. Part II: Wave breaking. *J. Atmos. Sci.*, **60**, 1448–1455.
- Vanderhoff, J. C., Nomura, K. K., Rottman, J. W., and Macaskill, C., 2008: Doppler spreading of internal gravity waves by an inertia-wave packet. *J. Geophys. Res.*, **113**, C05018, doi:10.1029/2007JC004390.
- Zaron, E. D., and Egbert, G. D., 2006: Estimating open-ocean barotropic tidal dissipation: The hawaiian ridge. *J. Phys. Oceanogr.*, **36**, 1019–1035.